Optimization of Ni/ZnZr Catalyst for Enhanced Syngas Yield in Catalytic Pyrolysis of Rice Straw

Lin Liu, Yucheng Fang, Rongyi Gao, and Jianfen Li *

To enhance the catalytic performance of nickel-based catalysts and improve their efficiency in biomass pyrolysis, a nickel-based catalyst supported on a ZnZr composite carrier was synthesized using the sol-gel method. The morphological changes of the catalyst before and after the reaction were observed using X-ray diffraction, scanning electron microscopy, nitrogen gas adsorption, temperature-programmed reduction, and other methods to analyze its catalytic performance. A series of experiments were conducted to explore the optimal conditions for the catalyst's gas production, including carrier material ratios, loading amounts, residence time, and reaction temperature. The bimetallic carrier of Zn and Zr provided a higher specific surface area, allowing the metallic nickel to enter its mesopores. The synergistic effect of the bimetallic system facilitated the catalytic activity of nickel, significantly enhancing gas production. The maximum CO and H_2 production were achieved at Zn/Zr = 6/4. The catalyst achieved an optimal gas yield of 507 mL/g at a residence time of 20 min and a reaction temperature of 800 °C, demonstrating strong stability.

*Contact information: School of Chemical and Environmental Engineering, Wuhan Polytechnic University, Wuhan 430023, China; *Corresponding author: whpulijfen@126.com*

INTRODUCTION

The overuse of fossil fuels has resulted in severe environmental pollution. According to the "Statistical Review of World Energy" published by British Petroleum in 2022, global primary energy consumption reached 595.15 EJ in 2021, with renewable energy consumption amounting to 39.91 EJ. Despite renewable energy currently constituting only a small fraction of total energy consumption, its growth rate has been remarkable. Biomass resources, as a form of renewable energy, present a promising solution to this crisis. Unlike fossil fuels, the CO_2 produced during biomass combustion is nearly equivalent to the amount of CO_2 absorbed during their growth processes, thus achieving a near carbon-neutral cycle (Hu and Gholizadeh 2019). Therefore, fostering the sustainable development and utilization of biomass not only substitutes fossil fuels and reduces greenhouse gas emissions but it also lowers production costs.

Among the various types of biomass, lignocellulosic biomass is a commonly used bioenergy feedstock. It is primarily composed of cellulose, hemicellulose, and lignin (Klinghoffer *et al.* 2012). The challenge of improving the utilization efficiency of biomass while avoiding pollution and waste has become the core issue in biomass utilization today. Direct combustion of biomass generates a significant number of byproducts and waste, causing considerable environmental pollution. To maximize the utilization efficiency of

this biomass and minimize pollution, several transformation methods have been developed, among which pyrolysis stands out (Chan *et al.* 2019; Hu and Gholizadeh 2019). The biofuels produced through pyrolysis are not only convenient for transportation but also significantly enhance subsequent performance and gasification processes. During pyrolysis, biomass feedstocks need to undergo pretreatment, such as mechanical compression and centrifugal grinding, to achieve a dense and well-dispersed state. Subsequently, biomass is subjected to thermal treatment in an oxygen-free environment, leading to the generation of three-phase reaction products: liquid (bio-oil), gas (pyrolysis gas), and solid (biochar). Various catalysts are commonly employed in the pyrolysis process to lower the energy barrier and enhance the tendency of the pyrolysis reactions, thereby meeting people's requirements. Among these catalysts, supported catalysts demonstrate relatively higher catalytic efficiency (Bhoi *et al.* 2020).

Research on biomass pyrolysis catalysts plays a crucial role in determining the efficiency of biomass pyrolysis. Currently, nickel and cobalt are widely used as the main catalyst components. Among them, nickel-based catalysts are the preferred catalysts for biomass pyrolysis due to their high activity and low cost (Wu *et al.* 2013; Shen 2015). Modifying nickel-based catalysts to achieve a larger contact surface area and improve stability and activity has long been utilized in biomass tar removal. However, under high-temperature pyrolysis conditions, nickel-based catalysts tend to aggregate and became deactivated. Extensive research has demonstrated that active metals and supports are key factors affecting catalyst performance, and modifications of nickel-based catalysts typically focus on the aspects of active metals and supports. Therefore, researchers have made significant efforts to modify nickel-based catalysts, enhance their performance, and reduce coking.

ZrO$_2$ shows promising potential as a catalyst support due to its unique interactions with electron distribution and active components. Research indicates that ZrO$_2$ prevents catalyst cooking and enhances coke gasification (Sun *et al.* 2015), which has been attributed to its low concentration of Lewis acid sites and excellent stability (Walker *et al.* 2012). The inclusion of ZnO in catalysts improves the activity and stability of CH$_4$ decomposition (Chen *et al.* 2008). Moreover, the addition of Zn to nickel-based catalysts enhances the dispersion of Ni. This effect is ascribed to the stronger tetrahedral coordination tendency between Zn^{2+} and O^{2-} on the support's surface, which is lacking in Ni^{2+}(Loricera *et al.* 2012). Ye *et al.* (2018) investigated the impact of acidity of Ni/MCM-41 catalysts on biomass gasification tar removal and found that catalysts with higher acidity could generate higher hydrogen yields without significant sintering after gasification at 800 °C. The increased acidity also slightly promoted the formation of coke on the catalyst. Wang *et al.* (2022) synthesized Ni-Zr catalysts doped with Mn and Al via a one-step method for methane dry reforming. The synergistic effect of Al and Mn with Zr improved the activity of methane dry reforming and reduced carbon deposition. Characterization results revealed that the synthesized catalysts possessed a higher concentration of strong basic sites, smaller crystal grain size, and higher oxygen adsorption, which contributed to their stability. The modification methods and principles of Zn for nickel-based catalysts have also been extensively studied. Lin *et al.* (2022) prepared supported Ni catalysts using the impregnation-reduction method and explored the relationship between active sites and reaction pathways in Ni-catalyzed CO$_2$ hydrogenation. The results demonstrated that alloying Ni with Zn altered the electronic structure and d-band center of Ni, weakened the interaction between Ni and CO/H$_2$, and selectively catalyzed the reverse conversion of steam to CO, exhibiting excellent CO selectivity.

In this study, Ni/ZnZr catalysts were synthesized using the sol-gel method for catalyzing the pyrolysis of rice straw into syngas. The influencing factors in catalytic pyrolysis were investigated, and catalytic pyrolysis experiments were performed under optimal conditions to evaluate the performance of the catalyst in biomass pyrolysis.

EXPERIMENTAL

Catalyst Preparation

The catalyst was synthesized using the sol-gel method to achieve a high dispersion of the active components. First, ZnZr supports of different proportions were prepared by mixing 1.82 g of zinc nitrate and 2.82 g of zirconium nitrate (taking Zn/Zr = 6/4 as an example) in a beaker containing deionized water. Subsequently, the calculated amount of citric acid, ethylene glycol, and zinc nitrate solution were added, and the mixture was stirred continuously. Once the solid had completely dissolved, it was transferred to an oil bath at 95 °C and heated for 2 to 3 h until a gel-like liquid formed. The sample was then oven-dried at 105 °C for 12 h, followed by a 2-h calcination at 400 °C, resulting in the production of fresh Ni/ZnZr catalyst. Using the same method, catalysts with different nickel loading amounts (0-10 wt%) were prepared.

The reagents used for catalyst preparation in this study included nickel nitrate, zinc nitrate, zirconium nitrate, citric acid, and ethylene glycol. Detailed information regarding the required reagents and equipment during the experimental process is in Table 1.

Biomass pyrolysis feedstock was obtained from farms around Wuhan. It was pretreated before the experiment. First, the collected rice straw was washed and thoroughly dried. It was then crushed and sieved. Finally, the sieved rice straw was dried in an oven at 105 °C for 48 h to remove the effect of moisture on the experimental results The proximate analysis and ultimate analysis of the raw material rice straw are shown in Table 2.

Catalyst Characterizations

The crystal structure of the catalyst was tested using the Rigaku SmartLab SE instrument. A suitable amount of powder sample was taken and tested using an X-ray diffractometer, scanning from 5° to 90° at a rate of 5°/min. Cu-Kα radiation was employed as the light source, with a voltage and current of 40 kV and 40 mA, respectively. Additionally, the peak positions in the XRD spectrum were determined by comparing with the data cards from the International Centre for Diffraction Data (JCPDS).

The specific surface area, pore volume, and average pore size of the catalyst were measured using the Micromeritics ASAP 2460. The sample was first subjected to vacuum degassing at 120 °C for 6 h, followed by N_2 adsorption-desorption isotherm measurement at 77 K. The specific surface area and pore size distribution of the sample were determined using the BET equation and BJH method, respectively.

The determination of the sample's surface morphology was carried out using the ZEISS Ge mini 300 instrument. A small amount of sample was directly mounted on a conductive adhesive, and then gold sputter-coated using the Oxford Quorum SC7620 sputter coater at a coating current of 10 mA. Subsequently, the sample morphology was imaged using the ZEISS Ge miniSEM 300 scanning electron microscope at an accelerating voltage of 3 kV. Energy-dispersive X-ray spectroscopy mapping was performed with an accelerating voltage of 15 kV and a SE2 secondary electron detector.

The reduction temperature of different metal phases in the catalyst was determined using the temperature-programmed reduction (TPR) method, which was conducted on the Microtrac BELCAT II instrument. The catalyst was dried and pre-treated by heating from room temperature to 300 °C at a rate of 10 °C/min under a helium flow (50 mL/min) for 1 h, followed by cooling to 50 °C and then introducing a 10% H_2/Ar mixed gas (50 mL/min) for 0.5 h. The desorption process was carried out by heating at a rate of 10 °C/min to 800 °C, and the reduction gas was detected using a thermal conductivity detector (TCD).

Table 1. Experimental Reagents and Equipment

Reagents/Instruments	Model/Purity	Manufacturer/Supplier
$Ni(NO_3)_2 \cdot 6H_2O$	Analysis pure	Sinopharm Chemical Reagents CO. Ltd.
$Zn(NO_3)_2 \cdot 6H_2O$	Analysis pure	Sinopharm Chemical Reagents CO. Ltd.
$Zr(NO_3)_4 \cdot 5H_2O$	Analysis pure	Sinopharm Chemical Reagents CO. Ltd.
$(CH_2OH)_2$	Analysis pure	Sinopharm Chemical Reagents CO. Ltd.
$C_6H_8O_7 \cdot H_2O$	Analysis pure	Sinopharm Chemical Reagents CO. Ltd.
Fixed bed pyrolysis ovens	BTF-1200C	Anhui BEQ Equipment Technology Co., Ltd.
Electric thermostatic blast drying ovens	DHG-9055A	Shanghai Yiheng Technology Instrument Co., Ltd.
Box type resistance furnace	KSL-1200X	Hefei Kejing Material Technology Co., Ltd.
X-ray diffractometer	SmartLab SE	Rigaku
Scanning electron microscope	Ge mini 300	ZEISS
Programmed temperature rise chemisorber	Bel Cata II	MicrotracBEL
Specific surface area analyser	ASAP 2460	Micromeritics
Infrared gas analyser	Gasboard-3100P	Hubei Ruiyi Automatic Control System Co.

Table 2. Proximate and Ultimate Analysis of Rice Straw

Sample	Ultimate Analysis (%)					Proximate Analysis (%)			
	C	H	O	N	S	M	A	V	FC
Rice straw	39.67	5.73	39.51	0.84	0.16	4.21	14.09	76.33	5.37

Activity Test

The experimental setup for the pyrolysis experiment consists of four components: the gas supply section, the pyrolysis reaction section, the gas collection section, and the gas processing and analysis section, as shown in Fig. 1. This apparatus was chosen for conducting relevant experiments on straw pyrolysis. Firstly, the straw and prepared catalyst are respectively placed in two quartz boats, which are then inserted into the quartz tube. Subsequently, the temperature of the tube furnace is programmed to increase at a rate of 20 °C/min until reaching the reaction temperature. The valve of the nitrogen gas cylinder is opened, and the valve opening is adjusted to allow N_2 to flow into the reaction vessel at a rate of 0.5 L/min, maintaining this condition for 30 min to establish an inert atmosphere in the system. Once heated to the reaction temperature, the furnace is pushed to the reaction

zone to initiate the pyrolysis reaction process. After the pyrolysis reaction is completed, the reactor is moved to one end for cooling, and the generated gases are collected into gas bags. Finally, the collected gas is introduced into an infrared gas analyzer for analysis. To ensure experimental accuracy and minimize errors, each experimental group is conducted three times, and the average value is calculated.
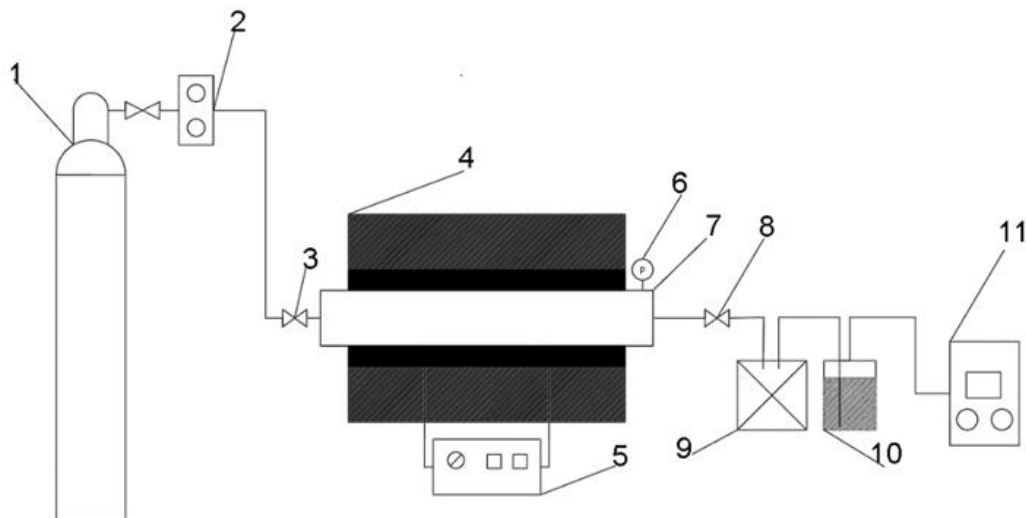
Fig. 1. Experimental setup diagram: 1-Nitrogen cylinder; 2-Rotor flow meter; 3-Tubular furnace inlet valve; 4-Electric furnace; 5-Temperature control program; 6-Pressure gauge; 7-Quartz tube; 8-Tubular furnace outlet valve; 9-Gas collection bag; 10-Gas treatment device; 11-Gas analyzer

RESULTS AND DISCUSSION

Characterization of Catalysts

To investigate the structural changes of the catalyst before and after its application, XRD characterization was performed on the fresh catalyst, as well as the catalysts used for 20 min and 100 min, as illustrated in Fig. 2. In the fresh catalyst sample, the diffraction peaks were barely discernible due to the efficient dispersion of metal particles, low crystallinity, and microcrystal sizes below the instrument's detection limit (Taherian *et al.* 2020). However, after 20 min and 100 min of usage, characteristic peaks corresponding to Ni_2O_3, ZrO_2, ZnO, and $NiZr$ were observed. The Ni_2O_3 peaks appeared at $2\theta=31.94°$ and $56.78°$ (JCPDS NO.14-0481), ZrO_2 peaks at $2\theta=30.24°$ and $50.25°$ (JCPDS NO.79-1770), ZnO peaks at $2\theta=34.50°$, $36.34°$, $47.65°$, $63.01°$, $68.12°$, and $69.26°$ (JCPDS NO.75-0576), and $NiZr$ peaks at $2\theta=42.82°$ and $60.37°$ (JCPDS NO.12-0478). By comparing the XRD patterns of the catalysts used for 20 min and 100 min, it was evident that with prolonged usage, the intensity of ZnO and Ni_2O_3 peaks decreased, while that of ZrO_2 slightly increased, and the intensity of $NiZr$ alloy peaks remained relatively stable. This indicates that the Ni species interacting with Zr had a certain degree of stability, while the characteristic peaks of the nickel oxide species had changed, showing that they gradually aggregated with increasing usage. Calculations using the Scherrer formula determined that the crystallite size of ZrO_2 in the catalyst used for 20 min was 10.3 nm, whereas in the catalyst used for 100 min, the ZrO_2 crystallite size increased to 18.2 nm. This suggests that as the catalyst is used for a longer duration, the degree of metal aggregation and the size of metal particles progressively increase.
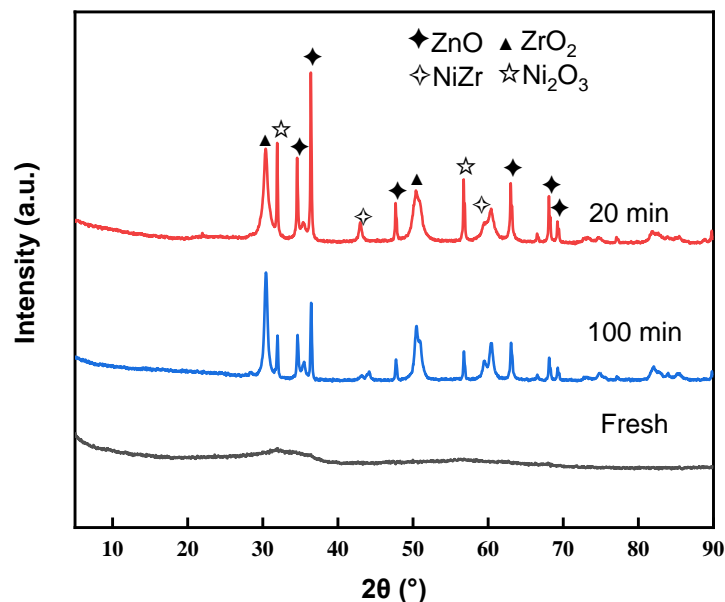
Fig. 2. XRD patterns of fresh catalyst and after use at different times

Table 3. Physical Properties of Fresh and Used Catalysts

Sample	S_{BET} (m^2/g)	Pore volume (cm^3/g)	Average pore diameter (nm)
Fresh	72.81	0.12	5.24
Used	181.91	0.12	3.04

Table 3 presents the physical characteristics of the catalyst before and after usage, along with the N_2 adsorption-desorption isotherms and pore size distribution plotted in Fig. 3. According to the classification by IUPAC, the fresh catalyst sample exhibited a Type IV isotherm, accompanied by a Type H1 hysteresis loop. Conversely, the catalyst after usage displayed a Type V isotherm and a Type H2 hysteresis loop. These results indicate that the fresh catalyst possessed cylindrical pores with the occurrence of mesopore capillary condensation (Taherian *et al.* 2020). In contrast, the used catalyst exhibited a connected pore effect, displaying narrower pore openings (Meirer *et al.* 2015). Furthermore, the specific surface area of the catalyst increased from 72.8 m^2/g to 182 m^2/g after usage. This significant increase can be attributed to the accumulation of Ni_2O_3 and ZnO nanoparticles during the pyrolysis reaction, as evidenced by the change from no peaks to peaks in the XRD spectra. (Fig. 2) (Yisup *et al.* 2005). By examining the pore size distribution of the catalyst, it was observed that the pore size distribution of the pre-used catalyst was relatively uniform, ranging from 2 to 30 nm. After usage, the pore size distribution extended from 2 to 50 nm, with a greater concentration in the range of 0 to 10 nm. The enlargement of pore size could be attributed to the collapse of interconnected smaller pores during the catalyst usage, resulting in the formation of larger pores. However, it is worth noting that this phenomenon only accounted for a small fraction, as most of the original pores experienced slight blockage, leading to a reduction in pore size. Importantly, the significant change in pore volume before and after catalyst usage may be attributed to the opposing effects of pore blockage, causing a decrease in pore volume, and pore collapse, resulting in an increase in pore volume, thereby offsetting each other. The decrease in average pore size in Table 3. further confirms the predominant occurrence of pore blockage.
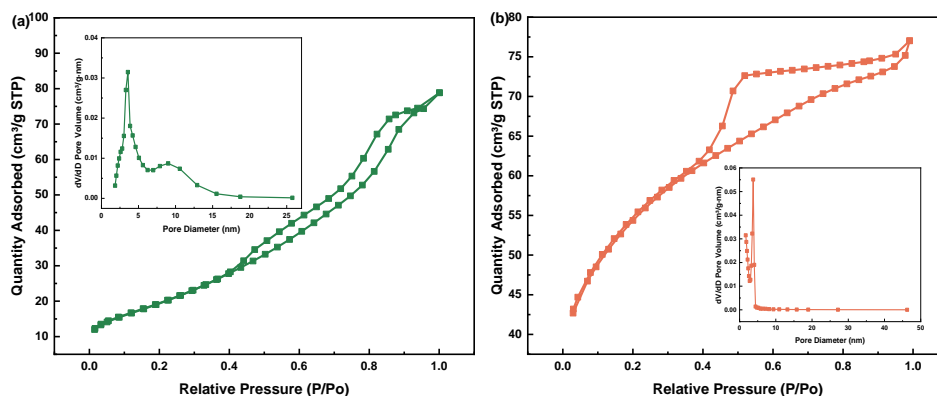
Fig. 3. Adsorption-desorption isotherms and pore size distribution of fresh and used catalysts: (a) fresh catalyst; (b) post-use catalyst

Figure 4 illustrates the surface morphology changes of the catalyst before and after usage. Upon comparative analysis, the surface morphology variations of the catalyst before and after usage were not significant. The fresh catalyst exhibited a porous structure (Feng *et al.* 2017) with a relatively smooth surface, showing minimal signs of agglomeration. However, numerous small particles were observed attached within the pores. After usage, the catalyst surface became rough, exhibiting various-sized agglomerated structures. These structures included metal agglomeration and carbon deposition. As indicated by the XRD analysis, the presence of metal oxides and Ni-Zr alloy confirms the phenomenon of metal accumulation. Moreover, these rough structures increased the specific surface area of the catalyst from 72.8 to 181.9 m^2/g. However, the carbon deposition covered some of the active metal sites, leading to a decrease in catalytic efficiency (Chen *et al.* 2004).
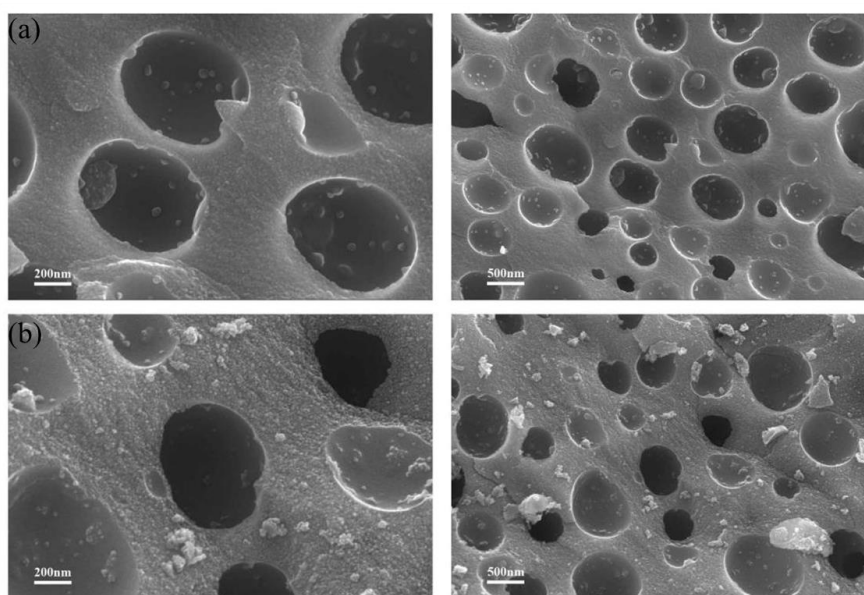
Fig. 4. SEM images of fresh and used catalysts: (a) fresh catalyst; (b) post-use catalyst

Figure 5 illustrates the hydrogen consumption curves of the samples after 20 min and 100 min (5 times) of usage. The 5%Ni/ZnZr catalyst subjected to thermal

decomposition for 20 min exhibited two distinct reduction peaks at 285 and 710 °C. These peaks correspond to the reduction of nickel oxide (285 °C) and nickel species strongly interacting with the ZnZr support (710 °C) (Valizadeh *et al.* 2022). It can be observed that the peak intensity of the reduction peak significantly decreased in the sample after 100 min of usage, and the reduction temperature shifted towards lower temperatures. Similarly, the reduction temperature of the nickel species interacting with the support also shifted towards the lower temperature range at 630 °C, making it easier to reduce, but with an increase in peak intensity(Li *et al.* 2012). The results showed that as the usage time increased, the nickel oxide particles on the catalyst surface decreased, leading to a reduction in the active nickel particles participating in the reaction. This caused the catalytic effect to decline. On the other hand, the growing interaction between the nickel species and the support led to an increase in hydrogen consumption. This indicates that prolonged high-temperature catalytic pyrolysis promotes the formation of more alloys between the active metal and the support, highlighting the pronounced phenomenon of metal agglomeration (Klinghoffer *et al.* 2012).
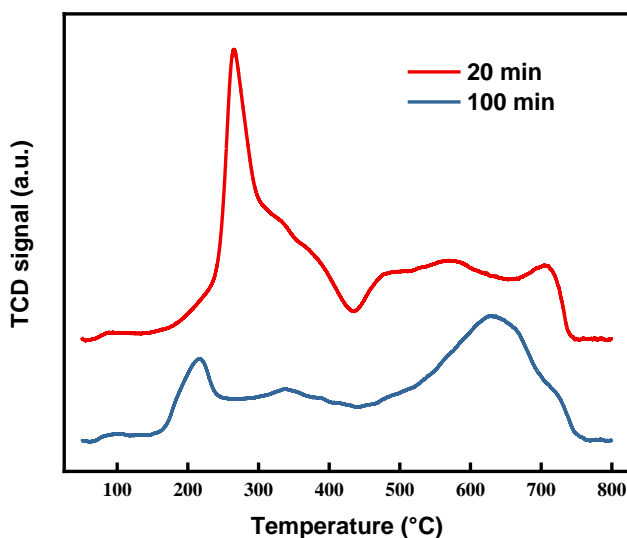
Fig. 5. H_2-TPR patterns of catalysts at different times after use

Effect of Carrier Ratio on Gas Yield

The catalyst's influence on the dispersion of the active components and regulation of the surface morphology is vital, thereby affecting the adsorption characteristics and reaction pathways of the catalyst (Shen *et al.* 2020). Consequently, the impact of metal supports with different proportions of ZnZr on the catalytic performance (without adding Ni) was investigated, as depicted in Fig. 6. Overall, the gas production efficiency of the two metal composites surpassed that of the single metal. The single metal exhibited gas production of approximately 400 mL/g, whereas the bimetallic catalyst achieved a minimum gas production of 506 mL/g (Zn/Zr=4/6) and a maximum of 536 mL/g (Zn/Zr=6/4), representing a gas production increase of 26.5% and 34.1% respectively. This indicates a synergistic effect between Zn and Zr in gas production (Raveendra *et al.* 2018). CO production demonstrated an increasing and then decreasing trend, with the highest production occurring at Zn/Zr=2/8 and 6/4, reaching approximately 192 mL/g. H_2 production follows a similar trend as CO, peaking at Zn/Zr=6/4 with a value of 202 mL/g. Compared to the absence of Zn, this represents a 64.89% increase in H_2 production, which

was initially 122 mL/g. However, the production of CO_2 and CH_4 was not significantly affected by changes on their production.
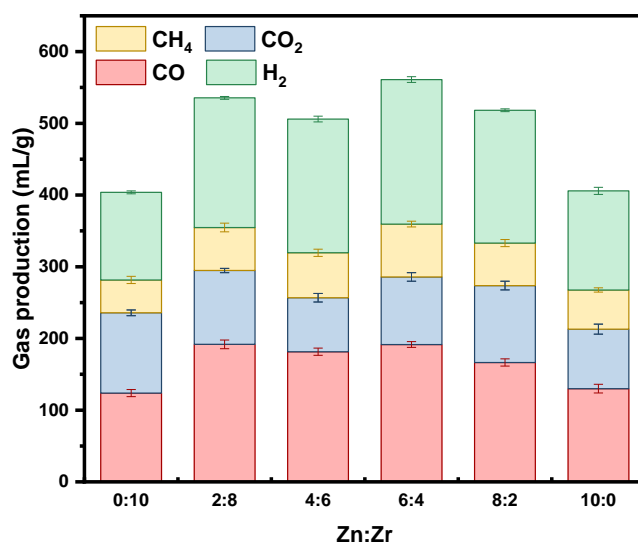
Fig. 6. Effect of different ZnZr ratios in the carrier on catalyst gas production

Effect of Nickel Loading on Gas Yield

Upon determining the appropriate support ratio, the influence of incorporating the active metal Ni on catalytic gas production was investigated, as depicted in Fig. 7.
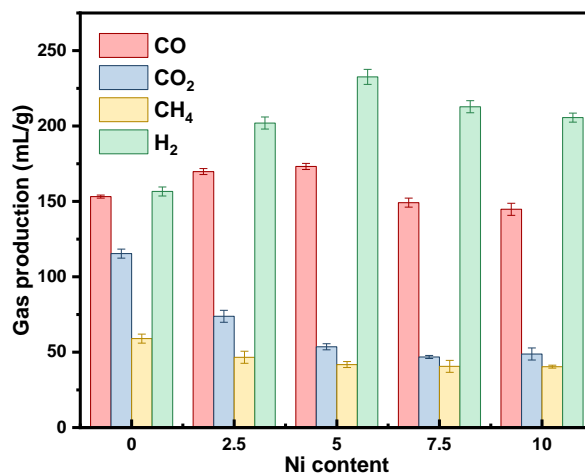
Fig. 7. Effect of different Ni levels on catalyst gas production

Generally, the addition of Ni resulted in increased H_2 production (Raveendra *et al.* 2018), surpassing 200 mL/g compared to the range of 153 mL/g without Ni. As the Ni content increases, H_2 production initially increased and then decreased. Particularly, the addition of 5% Ni yielded a peak H_2 production of 233 mL/g, representing a 51.8% increase compared to the baseline. However, the impact of Ni addition on CO production is limited, following a similar trend as H_2 production. At 5% Ni addition, CO production reached its maximum value of 173 mL/g, showing a mere 13.0% increase compared to the absence of Ni. These data collectively demonstrated the more significant impact of the active metal

Ni on catalytic hydrogen production. Regarding CO_2 and CH_4, their production demonstrates a decreasing trend. CH_4 production decreased by 31.5%, from 59.0 mL/g to 40.4 mL/g, while CO_2 production exhibited a more pronounced decrease, dropping by 57.7%, from 115 mL/g to 48.8 mL/g. Taking these factors into account, the addition of 5% Ni was judged to be the optimal choice (Zhang *et al.* 2018).

Effect of Residence Time on Gas Production

The residence time is one of the important factors determining the formation and distribution of products during pyrolysis. Increasing the residence time converts the organic vapors produced from lignocellulosic biomass into char and gas (Feng *et al.* 2020). Using the 5%Ni/ZnZr catalyst calcined at 400 °C, the influence of different residence times on gas product was studied, as shown in Fig. 8. With longer residence times, the gas production increased, and both CO and H_2 showed an upward trend. It is worth noting that the gas production increased from 10 min to 20 min. Specifically, the CO production increased from 148 to 216 mL/g, representing a 45.8% increase, while the H_2 production increased from 228 to 291 mL/g, representing a 27.3% increase. However, after 20 min, the increase in gas production becomes less pronounced, especially for H_2, which remained almost constant at 30 min compared to 20 min. This may be due to the increased formation of surface carbon and larger particle size of the metal catalyst with prolonged residence time, resulting in less noticeable improvement in catalytic efficiency. From 20 min to 40 min of pyrolysis, the CO production increased from 216 to 234 mL/g, representing a 7.8% increase, while the H_2 production increased from 291 to 301 mL/g, representing a 3.5% increase (Kan *et al.* 2016). On the other hand, both CO_2 and CH_4 decreased as the residence time increased. Although pyrolysis at 40 min produced more gas, it also consumed more energy, resulting in marginal improvement. From an economic perspective, a residence time of 20 min is preferable (Lovell *et al.* 2016).
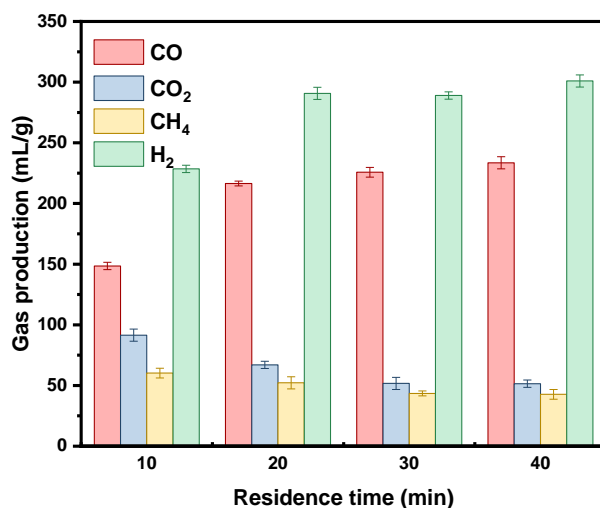
Fig. 8. Effect of residence time on catalyst gas production

Effect of Reaction Temperature on Gas Production

With a residence time of 20 min, the effect of pyrolysis temperature on gas products from rice straw using the 5% Ni/ZnZr catalyst was investigated, as shown in Fig. 9. At low temperatures (500 °C), the gas produced during pyrolysis was mainly composed of CO_2, accounting for nearly 40 vol.%. As the pyrolysis temperature increased, the CO_2

concentration gradually decreased, while the concentrations of CO and H_2 started to rise. The synthesis gas concentration increased from 48.8 vol.% (500 °C) to 81.0 vol.% (800 °C), representing a 32.2% increase. As for CH_4, due to its low production, its concentration fluctuated slightly, reaching its maximum at 600 °C. Increasing the pyrolysis temperature from 500 to 800 °C led to a significant increase in synthesis gas production, from 104 to 163, 298, and 507 mL/g, respectively. These values correspond to a relative increase of 56.5%, 187%, and 385% compared to the synthesis gas production at 500 °C. Comparatively, under the same temperature increment of 100 °C, the pyrolysis at 800 °C demonstrated superior performance. Xie *et al.* (2012) also found that higher gas yields were obtained in the range of 700 to 850 °C.
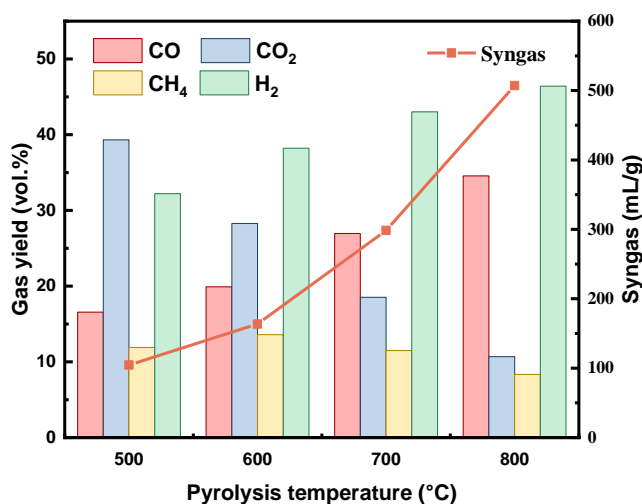
Fig. 9. Effect of pyrolysis temperature on catalyst gas production

Stability Test of Catalysts

The stability of catalysts has always been a matter of concern. Even after undergoing extensive thermal cycling, the catalyst should maintain its mechanical strength as well as high activity and selectivity (Liu *et al.* 2022). After determining all experimental conditions, a 5%Ni/ZnZr catalyst was selected and its cyclic stability was investigated during the catalytic biomass pyrolysis process, as shown in Fig. 10. Based on the experimental results, it was found that the initial gas production of the catalyst was 626 mL/g, with a synthesis gas yield of 507 mL/g. However, with an increasing number of uses, the gas production exhibited a gradual decline. This can be attributed to the accumulation of nickel and carbon species on the catalyst surface, as well as the formation of various metal oxides observed on the catalyst surface through XRD analysis. The BET characterization revealed an increase in specific surface area, but a decrease in catalytic efficiency, suggesting that this phenomenon may be due to the excessive carbon deposition, which covered the active sites of the catalyst (Li *et al.* 2003). After three cycles of catalyst usage, the catalytic activity became relatively stable, with a gas production of approximately 450 mL/g and a synthesis gas yield stabilizing at around 340 mL/g. In the absence of a catalyst, the total gas production was 342 mL/g, with a synthesis gas yield of 189 mL/g. After achieving stability, the total gas production of the catalyst still exhibited a remarkable enhancement of 31.7%, while the synthesis gas yield increased by 80.3%.

In summary, the sol-gel Ni/ZnZr catalyst demonstrates excellent performance for

rice straw pyrolysis under optimized conditions, holding great potential for biomass utilization. Further improving stability and antifouling ability is recommended.
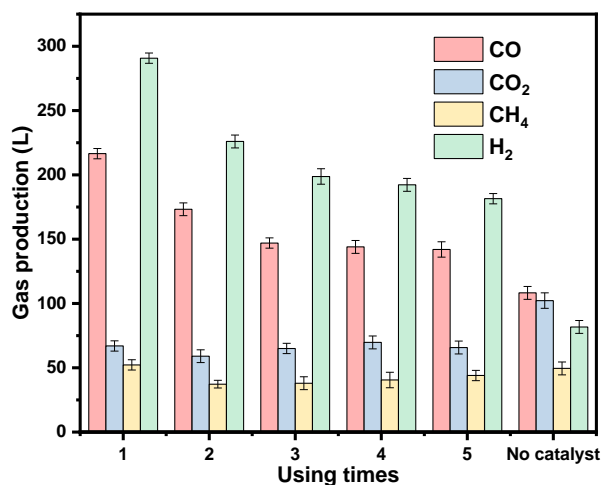
Fig. 10. Stability testing of catalysts

CONCLUSIONS

1. The ZnZr bimetallic carrier shows a synergistic effect in promoting gas yield compared to single metals, owing to the high specific surface area and Ni-support interaction.

2. Incorporating 5 wt.% Ni significantly increased the H_2 yield, while excessive Ni loading decreased gas production.

3. A residence time of 20 min gave the optimal gas yield. Further extension led to marginal improvements.

4. The catalyst exhibited declining activity after multiple uses due to carbon deposition and agglomeration, but it still enhanced syngas yield by 80.3% versus non-catalytic pyrolysis.

ACKNOWLEDGMENTS

REFERENCES CITED

Bhoi, P. R., Ouedraogo, A. S., Soloiu, V., and Quirino, R. (2020). "Recent advances on catalysts for improving hydrocarbon compounds in bio-oil of biomass catalytic pyrolysis," *Renewable and Sustainable Energy Reviews* 1(121), 13. DOI: 10.1016/j.rser.2019.109676

Chan, Y. H., Cheah, K. W., How, B. S., Loy, A. C. M., Shahbaz, M., Singh, H. K. G., Yusuf, N. R., Shuhaili, A. F. A., Yusup, S., Ghani, W., Rambli, J., Kansha, Y., Lam, H. L., Hong, B. H., and Ngan, S. L. (2019). "An overview of biomass thermochemical conversion technologies in Malaysia," *Science of the Total Environment* 1(680), 105-123. DOI: 10.1016/j.scitotenv.2019.04.211

Chen, H. W., Wang, C. Y., Yu, C. H., Tseng, L. T., and Liao, P. H. (2004). "Carbon dioxide reforming of methane reaction catalyzed by stable nickel copper catalysts," *Catalysis Today* 2-3(97), 173-180. DOI: 10.1016/j.cattod.2004.03.067

Chen, J. L., Qiao, Y. H., and Li, Y. D. (2008). "Promoting effects of doping ZnO into coprecipitated Ni-Al$_2$O$_3$ catalyst on methane decomposition to hydrogen and carbon nanofibers," *Applied Catalysis a-General* 2(337), 148-154. DOI: 10.1016/j.apcata.2007.12.007

Feng, P., Huang, K., Xu, Q., Qi, W., Xin, S., Wei, T., Liao, L., and Yan, Y. (2020). "Ni supported on the CaO modified attapulgite as catalysts for hydrogen production from glycerol steam reforming," *International Journal of Hydrogen Energy* 15(45), 8223-8233. DOI: 10.1016/j.ijhydene.2020.01.013

Feng, Y., Bin, D., Yan, B., Du, Y. K., Majima, T., and Zhou, W. Q. (2017). "Porous bimetallic PdNi catalyst with high electrocatalytic activity for ethanol electrooxidation," *Journal of Colloid and Interface Science* 1(493), 190-197. DOI: 10.1016/j.jcis.2017.01.035

Hu, X., and Gholizadeh, M. (2019). "Biomass pyrolysis: A review of the process development and challenges from initial researches up to the commercialisation stage," *Journal of Energy Chemistry* 1(39), 109-143. DOI: 10.1016/j.jechem.2019.01.024

Kan, T., Strezov, V., and Evans, T. J. (2016). "Lignocellulosic biomass pyrolysis: A review of product properties and effects of pyrolysis parameters," *Renewable and Sustainable Energy Reviews* 1(57), 1126-1140. DOI: 10.1016/j.rser.2015.12.185

Klinghoffer, N. B., Castaldi, M. J., and Nzihou, A. (2012). "Catalyst properties and catalytic performance of char from biomass gasification," *Industrial and Engineering Chemistry Research* 40(51), 13113-13122. DOI: 10.1021/ie3014082

Li, H. X., Luo, H. S., Zhuang, L., Dai, W. L., and Qiao, M. H. (2003). "Liquid phase hydrogenation of furfural to furfuryl alcohol over the Fe-promoted Ni-B amorphous alloy catalysts," *Journal of Molecular Catalysis a-Chemical* 1-2(203), 267-275. DOI: 10.1016/s1381-1169(03)00368-6

Li, X. C., Hu, Q. H., Yang, Y. F., Wang, Y., and He, F. (2012). "Studies on stability and coking resistance of Ni/BaTiO$_3$-Al$_2$O$_3$ catalysts for lower temperature dry reforming of methane (LTDRM)," *Applied Catalysis a-General* 1(413), 163-169. DOI: 10.1016/j.apcata.2011.11.004

Lin, S. X., Wang, Q., Li, M. S., Hao, Z. W., Pan, Y. T., Han, X. Y., Chang, X., Huang, S. Y., Li, Z. H., and Ma, X. B. (2022). "Ni-Zn dual sites switch the CO$_2$ hydrogenation selectivity via tuning of the d-band center," *ACS Catalysis* 6(12), 3346-3356. DOI: 10.1021/acscatal.1c05582

Liu, Y. J., Zuo, L. K., Zhou, Z. H., Zhang, J. H., Kang, Z. L., Zhu, J., and Zhu, G. X. (2022). "Ultrathin Ru-Ni nanounits as hydrogen oxidation catalysts with an alkaline electrolyte," *Dalton Transactions* 40(51), 15467-15474. DOI: 10.1039/d2dt02373c

Loricera, C. V., Castano, P., Infantes-Molina, A., Hita, I., Gutierrez, A., Arandes, J. M., Fierro, J. L. G., and Pawelec, B. (2012). "Designing supported ZnNi catalysts for the

removal of oxygen from bio-liquids and aromatics from diesel," *Green Chemistry* 10(14), 2759-2770. DOI: 10.1039/c2gc35901d

Lovell, E. C., Fuller, A., Scott, J., and Amal, R. (2016). "Enhancing Ni-SiO$_2$ catalysts for the carbon dioxide reforming of methane: Reduction-oxidation-reduction pre-treatment," *Applied Catalysis B-Environmental* 1(199), 155-165. DOI: 10.1016/j.apcatb.2016.05.080

Meirer, F., Kalirai, S., Morris, D., Soparawalla, S., Liu, Y. J., Mesu, G., Andrews, J. C., and Weckhuysen, B. M. (2015). "Life and death of a single catalytic cracking particle," *Science Advances* 3(1), 12. DOI: 10.1126/sciadv.1400199

Raveendra, G., Li, C. M., Bin, B., Cheng, Y., Meng, F. H., and Li, Z. (2018). "Synthesis of lower olefins from syngas over Zn/Al$_2$O$_3$-SAPO-34 hybrid catalysts: Role of doped Zr and influence of the Zn/Al$_2$O$_3$ ratio," *Catalysis Science and Technology* 14(8), 3527-3538. DOI: 10.1039/c8cy00574e

Shen, L., Xu, J., Zhu, M. H., and Han, Y. F. (2020). "Essential role of the support for nickel-based CO$_2$ methanation catalysts," *ACS Catalysis* 24(10), 14581-14591. DOI: 10.1021/acscatal.0c03471

Shen, Y. F. (2015). "Chars as carbonaceous adsorbents/catalysts for tar elimination during biomass pyrolysis or gasification," *Renewable and Sustainable Energy Reviews* 1(43), 281-295. DOI: 10.1016/j.rser.2014.11.061

Sun, F. M., Yan, C. F., Wang, Z. D., Guo, C. Q., and Huang, S. L. (2015). "Ni/Ce-Zr-O catalyst for high CO$_2$ conversion during reverse water gas shift reaction (RWGS)," *International Journal of Hydrogen Energy* 46(40), 15985-15993. DOI: 10.1016/j.ijhydene.2015.10.004

Taherian, Z., Khataee, A., and Orooji, Y. (2020). "Promoted nickel-based catalysts on modified mesoporous silica support: The role of yttria and magnesia on CO$_2$ methanation," *Microporous and Mesoporous Materials* 1(306), 8. DOI: 10.1016/j.micromeso.2020.110455

Valizadeh, S., Hakimian, H., Cho, E. H., Ko, C. H., Lee, S. H., Rhee, G. H., Jung, S. C., Yoo, K. S., and Park, Y. K. (2022). "Production of H$_2$-and CO-rich syngas from the CO$_2$ gasification of cow manure over (Sr/Mg)-promoted-Ni/Al$_2$O$_3$ catalysts," *International Journal of Hydrogen Energy* 88(47), 37218-37226. DOI: 10.1016/j.ijhydene.2021.12.176

Walker, D. M., Pettit, S. L., Wolan, J. T., and Kuhn, J. N. (2012). "Synthesis gas production to desired hydrogen to carbon monoxide ratios by tri-reforming of methane using Ni-MgO-(Ce,Zr)O-2 catalysts," *Applied Catalysis a-General* 1(445), 61-68. DOI: 10.1016/j.apcata.2012.08.015

Wang, Y., Li, L. I., Cui, C. J., Costa, P. D., and Hu, C. W. (2022). "The effect of adsorbed oxygen species on carbon-resistance of Ni-Zr catalyst modified by Al and Mn for dry reforming of methane," *Catalysis Today* 1(384-386), 257-264. DOI: 10.1016/j.cattod.2021.03.004

Wu, C. F., Dong, L. S., Onwudili, J., Williams, P. T., and Huang, J. (2013). "Effect of Ni particle location within the mesoporous MCM-41 support for hydrogen production from the catalytic gasification of biomass," *ACS Sustainable Chemistry and Engineering* 9(1), 1083-1091. DOI: 10.1021/sc300133c

Xie, Q. L., Kong, S. F., Liu, Y. S., and Zeng, H. (2012). "Syngas production by two-stage method of biomass catalytic pyrolysis and gasification," *Bioresource Technology* 1(110), 603-609. DOI: 10.1016/j.biortech.2012.01.028

Ye, M. J., Tao, Y. W., Jin, F. Z., Ling, H. J., Wu, C. F., Williams, P. T., and Huang, J. (2018). "Enhancing hydrogen production from the pyrolysis-gasification of biomass by size-confined Ni catalysts on acidic MCM-41 supports," *Catalysis Today* 1(307), 154-161. DOI: 10.1016/j.cattod.2017.05.077

Yisup, N., Cao, Y., Feng, W. L., Dai, W. L., and Fan, K. N. (2005). "Catalytic oxidation of methane over novel Ce-Ni-O mixed oxide catalysts prepared by oxalate gel-co-precipitation," *Catalysis Letters* 3-4(99), 207-213. DOI: 10.1007/s10562-005-2121-9

Zhang, Z. K., Liu, L. N., Shen, B. X., and Wu, C. F. (2018). "Preparation, modification and development of Ni-based catalysts for catalytic reforming of tar produced from biomass gasification," *Renewable and Sustainable Energy Reviews* 1(94), 1086-1109. DOI: 10.1016/j.rser.2018.07.010